EPJ manuscript No.
(will be inserted by the editor)

Zeeman energy and anomalous spin splitting in lateral GaAs quantum dots

Manuel Valín-Rodríguez[1] [a], Antonio Puente[1] and Llorenç Serra[1,2]

[1] Departament de Física, Universitat de les Illes Balears, E-07122 Palma de Mallorca, Spain
[2] Institut Mediterrani d'Estudis Avançats IMEDEA (CSIC-UIB), E-07122 Palma de Mallorca, Spain

March 8, 2004

Abstract. The level splittings induced by a horizontal magnetic field in a parabolic two-dimensional quantum dot with spin-orbit interaction are obtained. Characteristic features induced by the spin-orbit coupling are the appearance of zero-field gaps as well as energy splittings that depend on the electronic state and the orientation of the magnetic field in the quantum-dot plane. It is suggested that these quantum-dot properties could be used to determine the Rashba and Dresselhaus spin-orbit intensities

PACS. 73.21.La – 73.21.-b

1 Introduction

Nowadays, spin-related physics has become one of the most active branches of research in condensed matter. The fundamental physics involved and the potential applicability in semiconductor device technology constitute the main reasons encouraging this research. In particular, there is a special interest in the properties of electronic spins confined in a quantum dot. The reduced dimensionality of quantum dots makes them good candidates for systems sustaining long-lived spin states [1] and, ultimately, allowing coherent spin manipulation [2].

A most convenient way to distinguish spin states in a quantum dot fabricated within a two-dimensional electron gas (2DEG) is by means of a magnetic field. When the field is oriented parallel to the plane of the 2DEG it is expected that up and down spin directions will split by the Zeeman energy, with no additional modification of the electronic states. This assumption relies on the complete decoupling of the orbital motion and the parallel magnetic field. Since orbital motion is restricted to the 2DEG's plane, the vertical Lorentz force associated with a horizontal field becomes irrelevant. However, a qualitative difference appears when the electron feels an important spin-orbit (SO) interaction during its orbital motion. In this case the SO mechanism is effectively coupling the electronic states with the horizontal magnetic field, beyond a pure Zeeman splitting, even in two-dimensional dots.

Recently, several groups have measured the level splittings of lateral GaAs quantum dots in a parallel magnetic field [3,4], even for a single electron occupation of the dot. The measured splittings are usually interpreted in terms of an effective g-factor in a simple Zeeman formula. It is the aim of this work to analyze the theoretical prediction of level splittings for a quantum dot in a parallel magnetic field when SO interaction is present, emphasizing the deviations from the Zeeman scenario. It is also our purpose to discuss the possible SO signatures in the recent experimental data for single-electron dots [3,4].

[a] e-mail: vdfsmvr4@clust.uib.es

2 Quantum dot model

We consider a 2D representation of the effective mass Hamiltonian for the GaAs conduction-band electrons ($m^* = 0.067m_e$)

$$\mathcal{H}_{xy} = \frac{p_x^2 + p_y^2}{2m^*} + \frac{1}{2}m^*\omega_0^2(x^2 + y^2) \, . \tag{1}$$

The above hypothesis implies that the direction perpendicular to the 2DEG is strongly quantized in comparison with the in-plane degrees of freedom. The potential responsible for the confinement in the plane is taken as an isotropic parabola of constant ω_0. We also include the Zeeman energy

$$\mathcal{H}_Z = \frac{1}{2}g^*\mu_B \boldsymbol{B}\cdot\boldsymbol{\sigma} \, , \tag{2}$$

where $\boldsymbol{B} \equiv (B_x, B_y)$ and $\boldsymbol{\sigma} \equiv (\sigma_x, \sigma_y)$ are the magnetic field and the Pauli-matrix vectors, respectively; μ_B is the Bohr magneton and $g^* = -0.44$ is the bulk GaAs g-factor.

The SO interaction is taken into account by adding the linear Dresselhaus [5] and Bychkov-Rashba [6] terms for conduction band electrons in a [001] 2DEG [7],

$$\mathcal{H}_D = \frac{\lambda_D}{\hbar}(p_x\sigma_x - p_y\sigma_y) \, , \tag{3}$$

$$\mathcal{H}_R = \frac{\lambda_R}{\hbar}(p_y\sigma_x - p_x\sigma_y) \ . \tag{4}$$

These contributions originate, as a relativistic effect, in the electric fields present in the heterostructure. In their intrinsic reference frame, the moving electrons feel these electric fields as effective magnetic fields that interact with their spin. The Dresselhaus term is due to the bulk inversion asymmetry of the GaAs crystal and its intensity depends on the expectation value of the vertical momentum and a material-dependent constant ($\gamma = 27.5$ eVÅ^3 for GaAs) as

$$\lambda_D = \gamma\langle k_z^2\rangle \approx \gamma\left(\frac{\pi}{z_0}\right)^2 \ , \tag{5}$$

where z_0 is the vertical width of the 2DEG. On the other hand, the Rashba contribution stems from the asymmetry of the heterostructure profile (the built-in electric field) and it is also sensitive to the electric fields induced by external gates [8]. Below we shall treat λ_D and λ_R as varying parameters and study the results for different values. From Shubnikov-de Haas as well as magnetotransport measurements in 2DEG's values for these parameters ranging from ≈ 5 meVÅ to ≈ 50 meVÅ have been inferred in GaAs[9, 10].

Adding all the above contributions, the full Hamiltonian $\mathcal{H}$ can be considered as composed of two parts. The first one ($\mathcal{H}_0$), containing the kinetic energy, the confining potential and the SO interaction, remains invariant by the time-reversal symmetry. Conversely, the second part of the Hamiltonian, corresponding to the Zeeman term $\mathcal{H}_Z$, breaks this symmetry. More specifically, we have

$$\mathcal{H} = \mathcal{H}_0 + \mathcal{H}_Z \ , \tag{6}$$

$$\mathcal{H}_0 = \mathcal{H}_{xy} + \mathcal{H}_D + \mathcal{H}_R \ . \tag{7}$$

3 Analytical approximations

The analytical diagonalization of the full Hamiltonian is not available, although several analytical results can be obtained when different pieces of the Hamiltonian are neglected or treated within perturbation theory. The perturbative analysis when Zeeman and SO terms are of the same order of magnitude is rather involved and this case will be considered only numerically. In this section we shall consider the two limiting cases of zero Zeeman energy with a relatively weak SO interaction, and of a Zeeman energy much larger than SO effects.

Of course, another limit with analytical solution appears when the Zeeman energy is included and the SO interaction is switched off. Under these assumptions the Hamiltonian is trivial and its level structure is that of a two-dimensional oscillator

$$\varepsilon_{n\ell s} = (2n + |\ell| + 1)\hbar\omega_0 + \frac{1}{2}g^*\mu_B B s \ , \tag{8}$$

whose states are spin-split by the Zeeman energy gap $\Delta_s = |g^*|\mu_B B$, independently of the orbital state considered. In Eq. (8), $n = 0, 1, \ldots$ and $\ell = 0, \pm 1, \ldots$ are the principal and L_z quantum numbers, respectively, while $s = \pm 1$ is the spin label.

3.1 Limit of weak SO in zero field

Assuming $\mathcal{H}_Z = 0$ a perturbative calculation for $\mathcal{H}_{R,D} << \hbar\omega_0$ yields corrections of second order in the λ's and, due to the oscillator and spin degeneracies, requires degenerate perturbation theory. The modified energy levels read

$$\varepsilon_{n\ell s} = (2n + |\ell| + 1)\hbar\omega_0 - \frac{m^*}{\hbar^2}(\lambda_D^2 + \lambda_R^2) + \frac{m^*}{\hbar^2}(\lambda_D^2 - \lambda_R^2)\ell s \ . \tag{9}$$

The level structure given by Eq. (9) corresponds to that of a two-dimensional oscillator with a constant energy shift and a fine structure depending on ℓ and s. Both shift and splitting are proportional to the SO intensities. It is worth stressing that even in the present case of negligible Zeeman energy the SO interaction yields a spin-splitting of the energy levels given by $\Delta_s = 2\frac{m^*}{\hbar^2}\left|\,\ell(\lambda_D^2 - \lambda_R^2)\,\right|$. This zero-field splitting is consistent with the Kramers degeneracy present in a half-integer-spin system with time reversal symmetry. Indeed, each eigenstate characterized by the values of (n, ℓ, s) has a conjugate $(n, -\ell, -s)$ at the same energy.

An alternative method to derive Eq. (9) was suggested in Ref. [11] and uses a unitary transformation of $\mathcal{H}_0$ leading to a new Hamiltonian that is diagonal in spin space up to second order in the SO intensities. The remaining non-diagonal terms of $O(\lambda^3)$ are small compared with the diagonalized ones for typical GaAs λ's, and so they can be dropped without significant error. Using this alternative transformation we analyzed quantum dot properties like the far-infrared absorption in Ref. [12] and the spin precession in Ref. [13].

3.2 Limit of weak SO in large field

We assume now that there is a large horizontal field, such that $\mathcal{H}_{R,D} << \mathcal{H}_Z$. The unperturbed energy levels are those of Eq. (8), where up and down spin is defined in the direction of the magnetic field $\boldsymbol{B} \equiv B(\cos\theta, \sin\theta)$. As before, a second-order calculation within degenerate perturbation theory yields

$$\varepsilon_{n\ell s} = \varepsilon_{n\ell s}^{(0)} - \frac{m^*}{2\hbar^2}\left\{ G + F\frac{1}{1-z^2} \times \left[1 + s(2n + \ell + |\ell| + 1)z\right]\right\} \ , \tag{10}$$

where $\varepsilon_{n\ell s}^{(0)}$ is given by Eq. (8), and we have defined $z = g^*\mu_B B/\hbar\omega_0$, the ratio of Zeeman energy to external confinement frequency, as well as the two auxiliary quantities

$$G = \lambda_R^2 + \lambda_D^2 - 2\lambda_R\lambda_D\sin(2\theta) \ , \tag{11}$$

$$F = \lambda_R^2 + \lambda_D^2 + 2\lambda_R\lambda_D\sin(2\theta) \ . \tag{12}$$

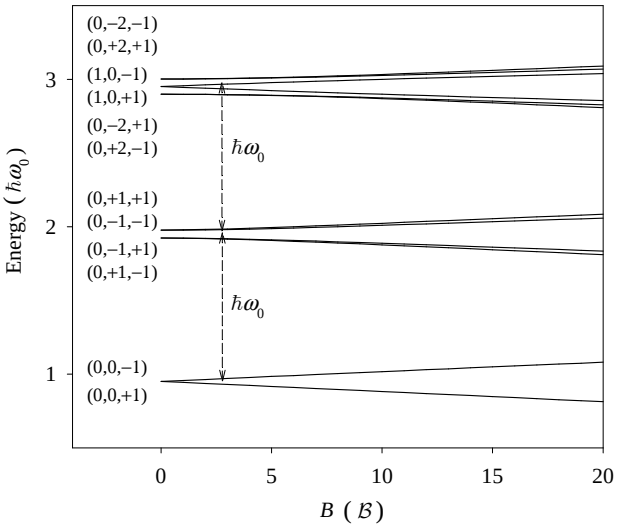

Fig. 1. Magnetic-field evolution of the first three oscillator shells of a parabolic quantum dot with SO interaction. The magnetic field is along the direction $\theta = 45$ deg and the SO intensities are $\lambda_D = 0.2\,\hbar\omega_0\ell_0$ and $\lambda_R = 0.1\,\hbar\omega_0\ell_0$. The labels indicate the values of (n, ℓ, s) for each $B = 0$ level (see text).

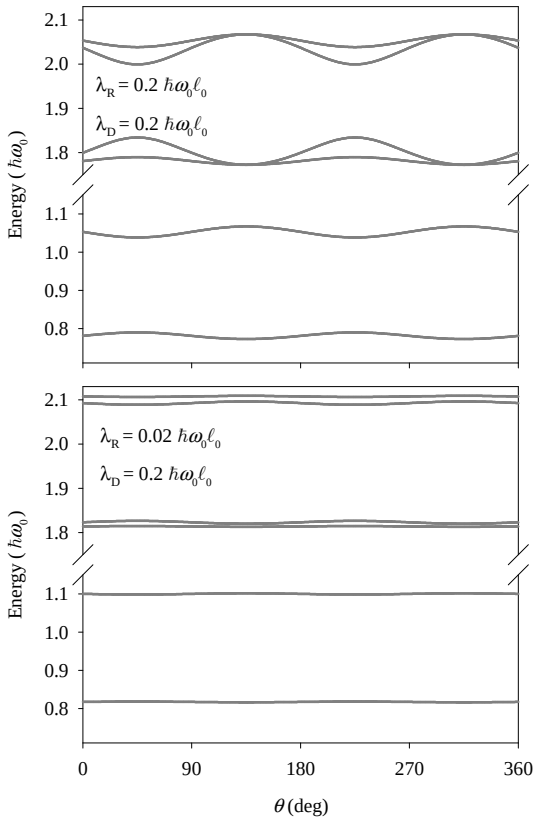

Fig. 2. Angular anisotropy of the first and second shells for a magnetic field of modulus $B = 20\mathcal{B}$ and the SO parameters displayed in each panel. The angle θ is the polar angle of the magnetic field vector.

In Eq. (10) the degeneracy of each major shell, with a given $N = 2n + |\ell|$, is broken into multiplets of states, as will be further clarified below when discussing the numerical results. It can be shown that the energies for $n = 0$, negative ℓ and $s = +1$ smoothly converge to the exact values for large enough magnetic fields. For other values of these labels there are discontinuities in the range of validity of Eq. (10) since an additional restriction is that the field, besides of being large enough, should not be close to a crossing point with an integer z. Note that Eq. (10) may actually diverge for $z = 1$. Another relevant feature of Eq. (10) is that it takes into account the angular anisotropy through the $\sin(2\theta)$ contribution to F and G.

It should be emphasized that although the energy levels from the above perturbative calculations, Eqs. (9) and (10), can still be classified using the uperturbed labels (n, ℓ, s), the corresponding states are no longer eigenstates of orbital and spin angular momenta. These results generalize those of Ref. [15] by including the two sources of SO coupling as well as the arbitrary angular orientation of the horizontal magnetic field.

4 Numerical solutions

As stated above, when both SO and Zeeman terms are included on the same footing a numerical resolution is required. We have used two alternative methods: a) by spatial discretization in a a uniform two-dimensional grid, and b) using an oscillator basis. In both methods we do not impose any symmetry restriction in either real or spin spaces and we have checked that the above analytical limits are recovered with high accuracy.

A natural unit system for the calculations is given by the parabola energy $\hbar\omega_0$ and the oscillator length $\ell_0^2 = \hbar/(m^*\omega_0)$. The associated unit of magnetic field is $\mathcal{B} = \omega_0 m^* c/e$ while the SO intensities are given in units of $\hbar\omega_0\ell_0$. Assuming, for instance, a GaAs parabolic dot with $\hbar\omega_0 = 1$ meV and $\lambda_D = 50$ meVÅ we would then have $\ell_0 \approx 338$ Å, $\mathcal{B} \approx 0.58$ T and, thus, $\lambda_D \approx 0.15\,\hbar\omega_0\ell_0$.

Figure 1 shows a typical dependence of a quantum dot's level structure with an applied horizontal magnetic field for the three lowest harmonic oscillator shells. The lowest subband corresponds to states having $(n = 0, \ell = 0, s = \pm 1)$ and it can be seen that these two states split linearly with the applied magnetic field, in a similar way to a usual Zeeman splitting.

The second subband is composed of four states characterized by $(n = 0, \ell = \pm 1, s = \pm 1)$. These states show a zero-field spin-splitting and at large fields they group into two branches, each of them composed of two almost parallel close lines. In the intermediate-field regime the evolution of these two branches is nonlinear with B. Note that the labels are given in the left part of the diagram according to the ordering of Eq. (9), which is appropriate to the $B = 0$ limit. At high B's the ordering, given by Eq. (10), changes since $s = +1$ (-1) corresponds to the lower (upper) branch.

The third subband includes both linear and non-linear splittings since this subband is composed of two states $(n = 1, \ell = 0, s = \pm 1)$ that split linearly with B, and

four states ($n = 0, \ell = \pm 2, s = \pm 1$) with a zero-field spin-splitting and a non-linear evolution. In general, at low fields states with $\ell = 0$ always split linearly with B (thus in a Zeeman-like way) while states having $\ell \neq 0$ do not split to first order in the field.

It can be easily checked that the the analytical approximations discussed in Sec. III reproduce the zero-field splittings and the fine-structured branches at large B in Fig. 1. The representation in this figure is a generalization to the parallel case of the well-known Fock-Darwin diagrams for quantum dots in perpendicular fields. When calculating this type of diagrams it is necessary to specify the orientation of the parallel magnetic field in the 2DEG plane since, in general, the anisotropy of the SO terms can reflect in an angular dependence of the level structure. However, there is one case where the level structure is fully isotropic and it is when only one source of SO coupling is present (Dresselhaus or Bychkov-Rashba). A general proof of this statement can be found in the following. Note, however, that the perturbative result Eq. (10) already predicts that the level structure is θ-independent when one of the two λ's vanishes.

If only one source of SO interaction is present in the Hamiltonian, its part preserving time reversal symmetry ($\mathcal{H}_0$) fulfills another continuous symmetry $\mathcal{S}$ with generator $\mathcal{G}$; i.e., $\mathcal{S} = e^{-i\theta\mathcal{G}/\hbar}$. For the Bychkov-Rashba and Dresselhaus cases it is $\mathcal{G} = L_z + S_z$ and $\mathcal{G} = L_z - S_z$, respectively. This result follows inmediately from the fact that both $\mathcal{H}_R$ and $\mathcal{H}_D$ commute with their corresponding symmetry generators. Taking into account that the energy levels of $\mathcal{H}$ and $\mathcal{S}^+\mathcal{H}\mathcal{S}$ are identical and that the latter corresponds in fact to a rotation of the magnetic field around a vertical axis and angle θ it follows that the level structure does not depend on the parallel field orientation. The transformed Hamiltonian indeed corresponds to a rotated field since

$$\begin{aligned}\mathcal{S}^+\mathcal{H}\mathcal{S} &= \mathcal{H}_0 + \frac{1}{2}g^*\mu_B\,\boldsymbol{B}\cdot\left(e^{i\theta S_z}\,\boldsymbol{\sigma}\,e^{-i\theta S_z}\right)\\ &= \mathcal{H}_0 + \frac{1}{2}g^*\mu_B\,\boldsymbol{B}_r\cdot\boldsymbol{\sigma}\ ,\end{aligned} \tag{13}$$

where $\boldsymbol{B}_r = (B_x\cos\theta + B_y\sin\theta, B_y\cos\theta - B_x\sin\theta)$ is the rotated field. This argument breaks down when both SO interaction sources are present since, then, the continuous symmetry $\mathcal{S}$ is lost and as a consequence, the level structure is anisotropic.

In agreement with the above discussion, the numerical calculations show that the angular anisotropy of the energy levels is maximal when $\lambda_R \sim \lambda_D$ and negligible when one SO intensity is much smaller than the other. This is clearly seen in Fig. 2, which displays the evolution with the magnetic field orientation of the levels corresponding to the lowest and the first-excited subbands of a dot in a parallel field $B = 20\mathcal{B}$. It is worth mentioning that not only the relative weight $\lambda_R/\lambda_D \sim 1$ yields an important anisotropy of the level structure. The abolute values are also relevant since, obviously, when both intensities are exceedingly smaller than $\hbar\omega_0\ell_0$ SO effects become negligible and the level structure is isotropic irrespectively of the relative weight. Another interesting feature is that the level anisotropy is sensitive to the relative sign of λ_R and λ_D. This is at variance with most physical properties, like the θ-averaged values of the energy levels, that are depending only on the absolute values $|\lambda_R|$ and $|\lambda_D|$. Focussing, for instance, on the first shell gap, we find from the numerical calculations that if $\lambda_R\lambda_D > 0$ the gap minima are at $\theta = \pi/4 + m\pi$ (with m an integer) while if $\lambda_R\lambda_D < 0$ the gap minima are shifted to $\theta = 3\pi/4 + m\pi$. In all cases, the anisotropy is characterized by a periodicity in 2θ, in agreement with the analytical formula derived above.

The detailed variation of the first-shell splitting with the SO intensities when $B = 20\mathcal{B}$ is summarized in Fig. 3. We note that for the chosen range of λ's the deviation of the θ-averaged splitting $\bar{\Delta}_s$ from the Zeeman value ($0.2948\hbar\omega_0$ at this B) ranges from 0 to $\approx 20\%$. The angular anisotropy (dashed lines) is measured by the difference between maximum and minimum energy gap, i.e., $[\max(\Delta_s(\theta)) - \min(\Delta_s(\theta))]$ and, in agreement with the above discussion, reaches maximum values along the diagonal line $|\lambda_R| = |\lambda_D|$, ranging from zero to $\approx 50\%$ of $\bar{\Delta}_s$. Figure 4 shows similar results for the splitting of the second-shell. Notice that in this more complex case we define two splittings: one gives the energy difference between the higher and lower states of the second shell while the other is associated with the two intermediate ones.

The numerical results in Fig. 3 qualitatively agree with the prediction from Eq. (10) of an averaged splitting and anisotropy proportional to $(\lambda_R^2 + \lambda_D^2)$ and $\lambda_R\lambda_D$, respectively. Nevertheless, the difference between the actual values from the second-order and numerical calculations increases with the λ's and it leads to sizeable errors for values above ~ 0.2. For the second-shell results (Fig. 4) the errors from the perturbative calculation are more conspicuous since they lead to qualitatively different contour lines for λ's above ~ 0.15.

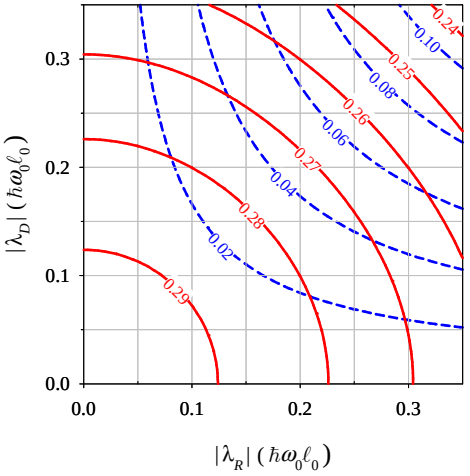

Fig. 3. Contour plots with the dependence on the spin-orbit intensities of the first shell-splitting at $B = 20\mathcal{B}$. Solid lines show the θ-averaged splitting $\bar{\Delta}_s$ in $\hbar\omega_0$ units (the Zeeman energy in these units is $E_Z = 0.2948$). Dashed lines correspond to the amplitude of the θ oscillation, $[\max(\Delta_s(\theta)) - \min(\Delta_s(\theta))]$.

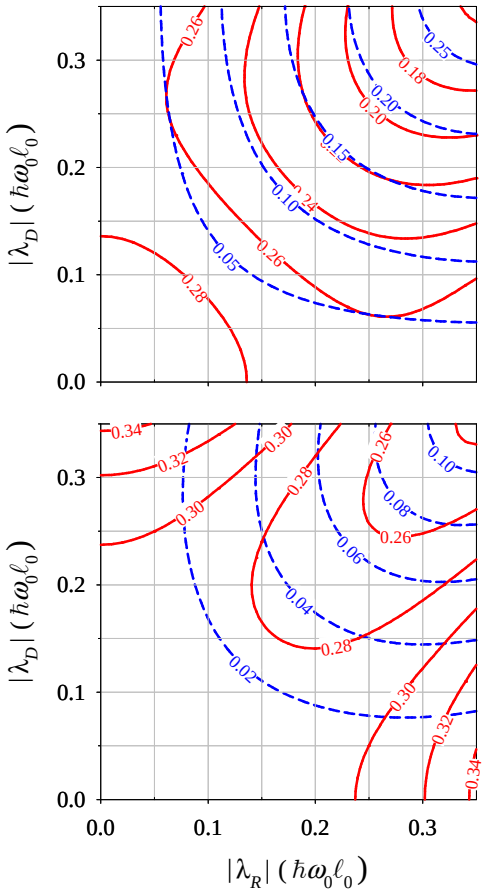

Fig. 4. Same as Fig. 3 for the second-shell splittings. Lower panel corresponds to the energy gap between higher and lower states, while upper panel shows the gap between the two intermediate ones.

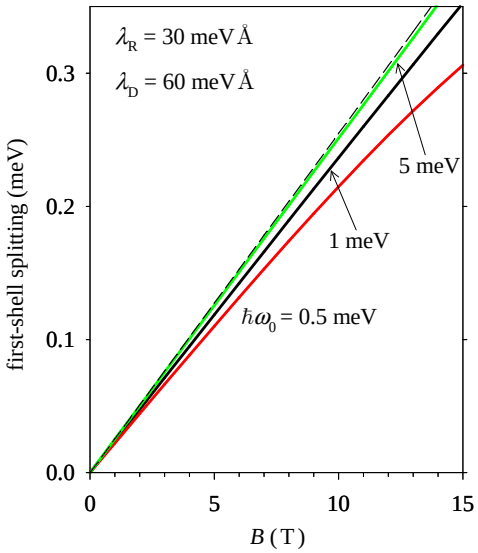

Fig. 5. Evolution with B of the lower shell splitting for fixed SO intensities and different values of the confinement $\hbar\omega_0$. The magnetic field orientation in the 2DEG's plane is given by a polar angle of $\theta = 45$ deg. The dashed line shows the Zeeman energy $|g^*|\mu_B B$.

The above results suggest that a high-precission measurement of the quantum dot level structure could determine the SO intensities. One should know the specific values of the underlying 2DEG (like g^* and m^*) as well as the value of ω_0. The zero-field splitting of the second shell would fix $|\lambda_D^2 - \lambda_R^2|$. This condition along with the results of the first-shell splitting at large B (Δ_s in Fig. 3) would yield the lower and greater SO intensities in absolute value, i.e., $|\lambda_<|$ and $|\lambda_>|$. The angular anisotropy of the splittings could fix, as mentioned above, the relative sign. To discern which source (Bychkov-Rashba or Dresselhaus) is the greater or lower SO intensity seems a somewhat complicate task. In principle, however, it could be accomplished by looking at the second shell splittings since when $|\lambda_D| > |\lambda_R|$ the upper (lower) states of the second shell have parallel (antiparallel) spin and orbital angular momenta at zero field.

The role of the orbital level spacing is quite important for understanding the B-evolution of the spin splittings when SO interaction is present. To see this, we display in Fig. 5 the lowest subband's splitting when the SO intensitites are kept constant and the confining frequencies are varied. Small dots, characterized by a wide gap between orbital subbands, show no effect of the SO interaction in this splitting, but, as the orbital and spin energy scales become comparable, due to the proximity of the orbital subbands, SO interaction induces a level repulsion that reflects in a compression of the levels reducing the spin splitting. For the particular λ's and magnetic field orientation in Fig. 5, the dots characterized by an orbital level spacing lower than ≈ 1 meV there is a sizeable reduction of the splitting with respect to the Zeeman value and thus their effective g-factor will be lower than that of the 2DEG.

The B-evolution corresponding to the second shell is more complex since, as already discussed above, this subband involves four different states. Figure 6 shows the two energy splittings corresponding to the gap between intermediate states and from the lowest to the highest one, respectively, of the second shell. In all cases, the evolution of the splittings is clearly non-linear showing a positive curvature at low B's and the above-mentioned finite value at zero field. It can be seen that as the orbital level spacing is reduced the values of the splittings at large B are also reduced due to the level repulsion induced by SO interaction, similarly to the case of the first subband. A very interesting feature is that for low enough $\hbar\omega_0$ the SO coupling induces a large separation of the two B-dependent gaps. A difference that does not appear in the case of small dots (high ω_0's) and, thus, it reveals the SO-induced fine structure of the dot level spectrum.

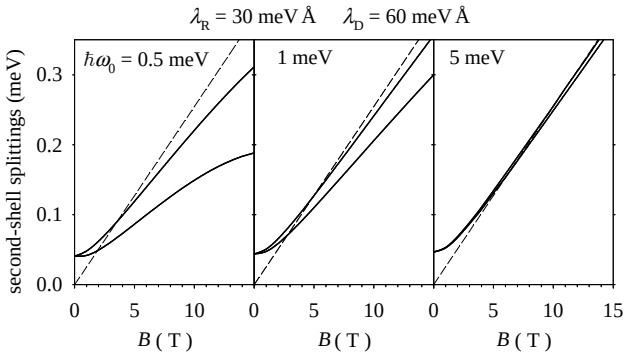

Fig. 6. Same as Fig. 5 for the energy splittings of the second shell. One splitting gives the energy gap between the highest and lowest states of this shell, while the other corresponds to the difference between the two intermediate states.

5 Discussion on experimental evidences and conclusions

In a recent work Potok *et al* [4] have measured the level structure and the corresponding spin splittings of the lowest and first-excited subbands for a GaAs lateral dot in a horizontal magnetic field (Fig. 2c of Ref. [4]). The data show a small deviation of the first-shell splitting at large $B_{\|}$ from the pure Zeeman result, with a fitted value of $|g| \sim 0.37$ (to be compared with 0.44 for the bulk). A single value of the second-shell splitting at large $B_{\|}$ is reported, since the resolution does not seem enough to discriminate finer structures. This second-shell energy gap is found to be somewhat lower than that of the first-shell. Unfortunately, the angular dependence is not discussed and the zero-field splitting of the second shell is not resolved, although the data suggest the existence of unresolved structures. The value of the confining frequency inferred from the level spacing is $\hbar\omega_0 \approx 0.8$ meV. As shown in Figs. 5 and 6, SO-induced effects for λ's in the range 30 to 60 meVÅ can reproduce the observations, but only for a selected magnetic field orientation. The corresponding angular anisotropies inferred from Figs. 3 and 4 are important and would reduce/enhance the difference from the pure Zeeman value when varying the polar angle θ.

Hanson *et al* [3] have also measured the spin-splitting of the first shell of a GaAs parabolic dot, this case evidencing a clear nonlinear $B_{\|}$-dependence (see Fig. 1e of Ref. [3]). The deviation from linear behavior is qualitatively similar to the $\hbar\omega_0 = 0.5$ meV results of Fig. 5 although the experimental value of $\hbar\omega_0$ at low $B_{\|}$'s is close to 1 meV. Therefore, to ascribe the observation to SO effects one should assume that the value of the confinement $\hbar\omega_0$ decreases as $B_{\|}$ increases[14].

In summary, we have analyzed the energy level structure and splittings that are predicted within the effective-mass model of a 2D parabolic quantum dot with Bychkov-Rashba and Dresselhaus SO interactions. The deviations from the simple Zeeman-splitting scenario have been stressed. Characteristic features of the SO interactions are the appearance of zero-field splittings, effective g-factors smaller than the bare one and sizeable anisotropies when both SO sources are of the same order. It has been suggested that these features could be used to determine the SO intensities from quantum dot measurements.

Spin-orbit intensities in the range of ≈ 50 meVÅ yield effects that are close to recent observations in GaAs quantum dots. However, a conclusive evidence allowing to validate or discard the relevance of the SO interaction for these measurements is lacking. In this respect, the clarification of the experimental zero-field splitting of the second shell as well as of the θ-dependence of the splittings would be very important.

This work was supported by Grant No. BFM2002-03241 from DGI (Spain).

References

1. A. V. Khaetskii and Y. V. Nazarov, Phys. Rev. B **64** 125316 (2001).
2. D. Loss and D. P. DiVincenzo, Phys. Rev. A **57** 120 (1998).
3. R. Hanson, B. Witkamp, L.M.K. Vandersypen, L.H. Willems van Beveren, J.M. Elzerman, and L.P. Kowenhoven, Phys. Rev. Lett. **91**, 196802 (2003).
4. R. M. Potok, J.A. Folk, C.M. Marcus, V. Umansky, M. Hanson, and A. C. Gossard, Phys. Rev. Lett. **91**, 016802 (2003).
5. G. Dresselhaus, Phys. Rev. **100**, 580 (1955).
6. Y.A. Bychkov and E. I. Rashba, J. Phys. C **17**, 6039 (1984).
7. W. Knap, C. Skierbiszewski, A. Zduniak, E. Litwin-Staszewska, D. Bertho, F. Kobbi, J. L. Robert, G. E. Pikus, F. G. Pikus, S. V. Iordanskii, V. Mosser, K. Zekentes, Yu. B. Lyanda-Geller, Phys. Rev. B **53**, 3912 (1996).
8. D. Grundler, Phys. Rev. Lett. **84**, 6074 (2000).
9. P. Ramvall, B. Kowalski, and P. Omling, Phys. Rev. B **55**, 7160 (1997).
10. J.B. Miller, D.M. Zumbühl, C.M. Marcus, Y.B. Lyanda-Geller, D. Goldhaber-Gordon, K. Campman, and A. C. Gossard, Phys. Rev. Lett. **90**, 076807 (2003).
11. I.L. Aleiner and V.I. Fal'ko, Phys. Rev. Lett. **87**, 256801 (2001).
12. M. Valín-Rodríguez, A. Puente, and Ll. Serra, Phys. Rev. B **66**, 045317 (2002).
13. M. Valín-Rodríguez, A. Puente, Ll. Serra, and E. Lipparini, Phys. Rev. B **66**, 235322 (2002).
14. M. Valín-Rodríguez, A. Puente, and Ll. Serra, Phys. Rev. B **69**, 085306 (2004).
15. M. Governale, Phys. Rev. Lett. **89**, 206802 (2002).